Radiation Physics and Chemistry 167 (2020) 108236

Contents lists available at ScienceDirect

Radiation Physics and Chemistry

journal homepage: www.elsevier.com/locate/radphyschem

Computational dosimetry in a pediatric i-CAT procedure using virtual anthropomorphic phantoms

Lucio P. Neves[a,b], Adriane B. Franco[c,b], Monique França[b], Maria R. Soares[d], Walmir Belinato[f], William S. Santos[a,e], Linda V.E. Caldas[e], Ana P. Perini[a,b,*]

[a] Instituto de Física, Universidade Federal de Uberlândia, Uberlândia, MG, Brazil
[b] Programa de Pós-Graduação em Engenharia Biomédica, Faculdade de Engenharia Elétrica, Universidade Federal de Uberlândia, MG, Brazil
[c] Faculdade Santa Rita de Cássia, Itumbiara, GO, Brazil
[d] Fundação Universidade Federal de Rondônia (UNIR), Porto Velho, RO, Brazil
[e] Instituto de Pesquisas Energéticas e Nucleares, Comissão Nacional de Energia Nuclear (IPEN-CNEN/SP), São Paulo, SP, Brazil
[f] Instituto Federal da Bahia (IFBA), Vitória da Conquista, BA, Brazil

ARTICLE INFO

Keywords:
Monte Carlo simulation
i-CAT
Pediatric dosimetry

ABSTRACT

The craniofacial structure is three-dimensional, and for a better visualization of these structures, Computed Tomography is often employed for diagnoses, even though being a high-cost procedure, leading to increased exposure to ionizing radiation. As a consequence, studies in dosimetry are necessary, since several radiosensitive structures are located in the head and neck, such as thyroid, crystalline and salivary glands. There is an overall consensus regarding the exposure of pediatric patients to ionizing radiation, with recommendations being that the procedures must occur with the shortest exposure time as possible, and it is only prescribed when they are effectively necessary. During the procedures, radiation effects are difficult to be measured. The use of either TL or OSL dosimeters can create artifacts within the images, and the positioning of a large number of dosimeters, necessary for the correct dose evaluation, is not feasible when it comes to a pediatric patient. Therefore pediatric virtual anthropomorphic phantoms and Monte Carlo simulations were used in this work. The absorbed and effective doses were determined during an i-CAT procedure, with 5 different fields of view, utilizing 5- and 10-year-old male virtual anthropomorphic phantoms. The results pointed out that the eye lens, salivary glands and thyroid received the highest doses. Besides, the effective dose values increase with the increasing of the FOV size, and the 5-year-old male virtual anthropomorphic phantom presented the highest effective dose values.

1. Introduction

Radiology is a major procedure mainly used for diagnostic concerns within patients, such as trauma, fractures, and genetic malformations. Conventional diagnostic radiology is performed through the use of ionizing radiation, being conventional X-rays, mammography and computed tomography (CT) scans the most common examples. Among the CT scans, there is one often used, the cone beam CT (CBCT), which was originally created for angiography usage (Robb, 1982), but has its use expanded for other areas, such as radiotherapy treatment planning (Cho et al., 1995), mammography (Chen and Ning, 2002) and orthodontics (Hatcher and Aboudara, 2004), a speciality of dentistry.

CBCT consists in acquiring images through the use of ionizing radiation emitted by a centralized beam of X-rays, in a conical format, generating two-dimensional images of the patient. The output has its dimensions reconstructed through algorithms, providing a three-dimensional image. The use of CBCT in orthodontics is in constant growth (Hatcher and Aboudara, 2004; Guerrero et al., 2006), since anatomical analyses are possible (Vos et al., 2009).

CBCT provides images of high diagnostic quality, with radiation doses lower than other CT scans (Mischkowski et al., 2007). Considering the mandible examination, the voxel size edge on an i-CAT scanner is approximately between 0.12 and 0.4 mm, and for a conventional CT method the voxel size edge is from 0.5 to 1.0 mm (Torres et al., 2010).

Given all its advantages, CBCT has a great acceptance in orthodontics (Kapila et al., 2011; Guerrero et al., 2006). It produces three-dimensional images of the facial skeleton and the dental arcade of

* Corresponding author. Instituto de Física, Universidade Federal de Uberlândia, Uberlândia, MG, Brazil.
E-mail addresses: lucio.neves@ufu.br (L.P. Neves), adriane.franco@ufu.br (A.B. Franco), franca_monique@ufu.br (M. França), mrs@unir.br (M.R. Soares), walmir@ifba.edu.br (W. Belinato), william@ufu.br (W.S. Santos), lcaldas@ipen.br (L.V.E. Caldas), anapaula.perini@ufu.br (A.P. Perini).

https://doi.org/10.1016/j.radphyschem.2019.03.040
Received 15 December 2018; Received in revised form 23 March 2019; Accepted 26 March 2019
Available online 29 March 2019
0969-806X/

patients. According to the results presented in the study of Vos et al. (2009), 41% of maxillofacial surgeries, 29% of dentoalveolar pathology diagnoses, 16% of orthodontic procedures and 11% of dental implant plans, use CBCT. Such fact might have been influenced by an important detrimental effect caused by CT scans. There have been several studies (Schulze et al., 2004; Scaf et al., 1997; Dula et al., 1997) showing that it delivers a radiation dose of about 2000 μSv to the patients, due to the radiological examination of the maxillofacial region by conventional CT. In opposition to that, after applying the CBCT method, there has been a dose reduction from 76.2% to 98.5% as reported by Scarfe and Farman (2008).

Therefore, this dose reduction in CBCT (Alkhader et al., 2010; Wall et al., 2006), encouraged its use with pediatric patients. Some os these usages includes: analysis in anatomically difficult sites; in lips and palate clefts analyses, due to this more precise images, increasing surgery and rehabilitation easiness of patients; as well as in impacted teeth suspicion and supernumerary teeth (Dhillon and Kalra, 2013).

Although delivering relatively low doses, CBCT still deposits energy through the diagnosis method. Therefore, when performed in children, the risks are higher. The main explanation for that is because the tissue and organs of children are more radiosensitive than of adults (Najjar et al., 2013; Pierce and Preston, 2000; Huda et al., 1997; Hall and Giaccia, 2006). In addition, the probability of cancer occurrence is greater in children (Berdon, 1999), since their life span is considered longer (Whaites, 2006), and thus more time for the cancer appearance. This fact points the necessity of dosimetric studies with children (Papadimitroulas et al., 2018).

The occurrence estimation of stochastic effects, such as carcinogenesis, is proportional to an age-based multiplication factor. For example, children under the age of 10 have a 3-degree factor, while in adults at the ages ranging from 30 to 50 years corresponds to 0.5 (Smith-Bindman et al., 2009). Therefore, it can be inferred that the difference in radiation sensitivity between children and adults is from 2 to 3 times greater for pediatric patients (Brenner et al., 2001). Given this context, the CBCT for pediatric dentistry should be applied with caution, and in either extremely necessary, or in non-routine situations (Theodorakou et al., 2012). It is also important to consider that the exposure of pediatric patients to ionizing radiation has to be as low as possible (Theodorakou et al., 2012) to obtain acceptable images for clinical use.

Theodorakou et al. (2012) studied the biological effects of radiation due to CBCT in two groups: 5-year-old children and adolescents. The evaluation consisted of getting the same radiation dose in both groups, being only different with the amount of absorbed dose, because it depends on the size and the shape of the patients. The researchers found that the thyroid gland of the 5-year-old child's group, for example, absorbed 4 times more dose than the adolescent ones. There have been several studies relating CBCT in dental exams, using thermoluminescent dosimeters (TLD) with phantoms (Okano et al., 2009; Ludlow and Ivanovic, 2008; Ludlow et al., 2006; Tsiklakis et al., 2005; Roberts et al., 2008). Even though not being comparable in many ways, such as using different simulator objects (composed of several distinct materials), different TLD models, quantities and positioning schemes, such results emphasized the protection against ionizing radiation, especially for children (Okano et al., 2009; Ludlow and Ivanovic, 2008; Ludlow et al., 2006; Tsiklakis et al., 2005; Roberts et al., 2008).

Studying the radiation-based diagnosis doses is important, once getting the lowest risk with highest visualization potential must be the target. Therefore, a different analysis is through the usage of the Monte Carlo method (MC), which is a fundamental tool in calculating deposited energy and absorbed dose (Kramer et al., 1982). There are also virtual tools such as the anthropomorphic phantoms, which can be mathematical or voxel based (ICRP Publication 110, 2009; Cassola et al., 2010a; Lima et al., 2011; Lee et al., 2010). Such virtual anthropomorphic phantoms, representing the anatomy of the human body, consider the different locations, like the pulmonary, adipose, soft and bone tissues (Lima et al., 2011; Lee et al., 2010; Cassola et al., 2010b; Norris et al., 2014).

The present study aims to evaluate the radiation doses in the CBCT examinations in pediatric dentistry using the i-CAT scanner, in children at the age of 5 and 10. Pediatric anthropomorphic phantoms (Lima et al., 2011) were used, representing the characteristics of the tissues of the children's maxillofacial region, as well as the Monte Carlo computational code (Pelowitz, 2011), to obtain the absorbed and effective doses.

2. Materials and methods

2.1. Cone beam computed tomography device

In this work the i-CAT CBCT classical equipment, manufactured by Imaging Sciences International (2010) was employed in the simulations. This equipment has 5 different fields of view (FOV) sizes (diameter × height): 8 cm × 6 cm, 14 cm × 6 cm, 14 cm × 8 cm, 14 cm × 13 cm, and 14 cm × 22 cm. During an examination the gantry rotates 360° around the patient, and the parameters utilized were: tube voltage of 120 kV and anodic current of 5 mA. The exam provides 215 two-dimensional images, in a time of 40 s, for further 3D reconstruction.

2.2. Male pediatric virtual anthropomorphic phantoms

In order to perform a study of radiation doses under CBCT analysis through i-CAT scanners, the present study used the mesh generation virtual pediatric anthropomorphic phantoms (Lima et al., 2011), which represents the anatomy and dimensions of the 5- and 10-year-old male children, according to the International Commission on Radiological Protection (ICRP Publication 89, 2002). They were developed at the *Department of Nuclear Energy of the Federal University of Pernambuco* (Lima et al., 2011). The phantoms positioned on the i-CAT equipment are presented in Fig. 1. The virtual pediatric anthropomorphic phantoms present the following characteristics:

5-year-old virtual anthropomorphic phantom: body mass of 19.13 kg, height of 1.09 m, matrix (columns × lines × slices): 284 × 143 × 780 and voxel dimensions (mm^3) of 1.4 × 1.4 × 1.4.

10-year-old virtual anthropomorphic phantom: body mass of 32.34 kg, height of 1.38 m matrix (columns × lines × slices): 353 × 157 × 987 and voxel dimensions (mm^3) of 1.4 × 1.4 × 1.4.

2.3. Monte Carlo simulation

The radiation dose calculations were performed through the MCNPX radiation transport code that uses the Monte Carlo technique.

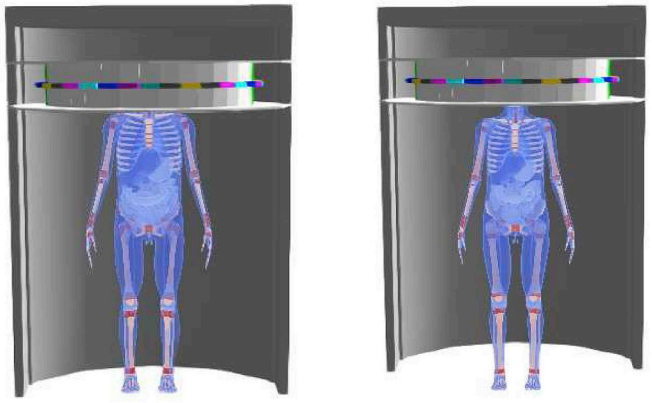

Fig. 1. (A) 5-year-old male virtual anthropomorphic phantom and (B) 10-year-old male virtual anthropomorphic phantom positioned on the i-CAT equipment.

Table 1
Absorbed and effective doses determined for a 5-year-old male pediatric virtual anthropomorphic phantom in an i-CAT exam, for several FOV sizes and a 120 kVp tube voltage. Remainder Tissues are: Adrenals, Extratoracic region, Gall bladder, Heart, Kidneys, Lymphatic nodes, Muscle, Oral mucosa, Pancreas, Ovaries, Small intestine, Spleen, Thymus and Uterus. The uncertainties are presented in parenthesis (in %).

Organs	Absorbed doses (mGy) for different FOV sizes (cm × cm)				
	8 × 6	14 × 6	14 × 8	14 × 13	14 × 22
Red bone-marrow	1.6E-01 (0.05)	2.4E-01 (0.04)	2.5E-01 (0.03)	2.6E-01 (0.03)	2.7E-01 (0.02)
Colon	3.2E-03 (1)	4.4E-03 (1)	4.3E-03 (1)	4.6E-03 (1)	6.8E-03 (0.4)
Lung	1.2E-01 (0.1)	1.6E-01 (0.1)	1.8E-01 (0.1)	2.6E-01 (0.06)	4.5E-01 (0.03)
Stomach	1.3E-02 (1)	1.9E-02 (1)	2.0E-02 (0.6)	2.3E-02 (0.4)	3.8E-02 (0.3)
Breast	6.2E-01 (0.2)	8.9E-01 (0.2)	1.1E + 00 (0.1)	1.3E + 00 (0.1)	1.1E + 00 (0.1)
Remainder tissues	9.5E-03 (0.04)	1.4E-02 (0.03)	1.3E-02 (0.03)	1.3E-02 (0.02)	1.4E-02 (0.02)
Gonads	1.8E-03 (11)	2.0E-03 (10)	1.6E-03 (10)	1.2E-03 (9)	1.0E-03 (7)
Bladder	9.2E-04 (5)	1.1E-03 (4)	1.1E-03 (4)	1.1E-03 (3)	1.5E-03 (2)
Oesophagus	3.1E-01 (0.3)	4.2E-01 (0.3)	4.9E-01 (0.2)	6.3E-01 (0.1)	7.3E-01 (0.1)
Liver	2.1E-02 (0.4)	3.0E-02 (0.4)	3.2E-02 (0.3)	3.7E-02 (0.2)	6.1E-02 (0.1)
Thyroid	2.0E + 00 (0.2)	2.5E + 00 (0.2)	2.9E + 00 (0.2)	3.2E + 00 (0.1)	2.5E + 00 (0.1)
Bone surface	2.4E-01 (1)	2.4E-01 (0.04)	2.5E-01 (0.03)	2.6E-01 (0.03)	2.7E-01 (0.02)
Brain	1.5E-01 (0.1)	2.2E-01 (0.1)	2.5E-01 (0.1)	3.8E-01 (0.05)	6.7E-01 (0.03)
Salivary glands	9.4E-01 (0.1)	1.2E + 00 (0.1)	1.1E + 00 (0.1)	8.1E-01 (0.05)	5.2E-01 (0.04)
Skin	1.8E-01 (0.04)	2.7E-01 (0.03)	2.7E-01 (0.03)	2.8E-01 (0.02)	2.8E-01 (0.02)
Eyes	1.3E-01 (1)	2.0E-01 (0.4)	2.3E-01 (0.4)	5.3E-01 (0.2)	1.1E + 00 (0.1)
Eye Lens	1.1E-01 (2)	1.8E-01 (1)	2.0E-01 (1)	4.8E-01 (1)	1.1E + 00 (0.3)
Effective dose (μSv)	218.7 (0.6)	297.1 (0.4)	336.4 (7)	394.9 (7)	376.7 (7)

Table 2
Absorbed and effective doses determined for a 10-year-old male pediatric virtual anthropomorphic phantom in an i-CAT exam, for several FOV sizes and a 120 kVp tube voltage. Remainder Tissues are: Adrenals, Extratoracic region, Gall bladder, Heart, Kidneys, Lymphatic nodes, Muscle, Oral mucosa, Pancreas, Ovaries, Small intestine, Spleen, Thymus and Uterus. The uncertainties are presented in parenthesis (in %).

Organs	Absorbed doses (mGy) for different FOV sizes (cm × cm)				
	8 × 6	14 × 6	14 × 8	14 × 13	14 × 22
Red bone-marrow	1.6E-02 (0.04)	2.4E-02 (0.04)	2.4E-02 (0.03)	2.5E-02 (0.02)	2.6E-02 (0.02)
Colon	1.5E-03 (2)	1.9E-03 (1)	1.8E-03 (1)	1.6E-03 (1)	2.0E-03 (1)
Lung	4.4E-02 (0.2)	6.5E-02 (0.2)	6.8E-02 (0.1)	8.3E-02 (0.1)	1.6E-01 (0.05)
Stomach	5.6E-03 (1)	7.9E-03 (1)	7.9E-03 (1)	8.2E-03 (1)	1.2E-02 (0.4)
Breast	4.2E-04 (0.2)	5.9E-04 (0.2)	6.7E-04 (0.2)	7.4E-04 (0)	6.0E-04 (0.1)
Remainder tissues	7.4E-02 (40)	1.1E-01 (35)	1.1E-01 (31)	9.9E-02 (26)	9.6E-02 (19)
Gonads	2.3E-03 (10)	2.3E-03 (10)	1.7E-03 (10)	1.2E-03 (9)	8.3E-04 (8)
Bladder	6.3E-04 (5)	7.1E-04 (5)	6.1E-04 (4)	5.0E-04 (4)	4.7E-04 (3)
Oesophagus	1.1E-01 (0.5)	1.6E-01 (0.4)	1.8E-01 (0.3)	3.0E-01 (0.2)	5.3E-01 (0.1)
Liver	8.4E-03 (1)	1.2E-02 (1)	1.2E-02 (0.4)	1.3E-02 (0.3)	1.7E-02 (0.2)
Thyroid	5.9E-01 (0.3)	7.6E-01 (0.3)	9.9E-01 (0.2)	1.9E + 00 (0.1)	2.3E + 00 (0.1)
Bone surface	1.4E-01 (13)	2.9E-03 (0.1)	2.9E-03 (0.04)	3.1E-03 (0.03)	3.3E-03 (0.03)
Brain	2.1E-01 (0.1)	3.0E-01 (0.1)	3.4E-01 (0.1)	4.7E-01 (0.1)	7.1E-01 (0.03)
Salivary glands	8.4E-01 (0.1)	1.2E + 00 (0.1)	1.1E + 00 (0.1)	8.2E-01 (0.04)	5.2E-01 (0.04)
Skin	1.2E-01 (0.04)	2.0E-01 (0.03)	2.0E-01 (0.02)	2.0E-01 (0.02)	1.9E-01 (0.02)
Eyes	1.8E-01 (0.4)	2.8E-01 (0.4)	3.5E-01 (0.3)	8.3E-01 (0.1)	1.2E + 00 (0.1)
Eye Lens	6.6E + 00 (0.4)	1.0E + 01 (0.4)	1.3E + 01 (0.3)	3.0E + 01 (0.1)	4.3E + 01 (0.1)
Effective dose (μSv)	58.9 (9)	79.3 (8)	88.7 (9)	128.9 (11)	165.5 (12)

This can be used in several transport modes: only neutron (mode n), photon (mode p), electrons (mode e), combination of photons and electrons (mode p, e), among others. The range of energies for photons is 1 keV–100 GeV, and for electrons it is 1 keV to 1 GeV (Pelowitz, 2011).

The simulation validation of the CBCT equipment was carried out in the work of Soares et al. (2019). In that work a new methodology was developed to determine the doses in dental CBCT from air kerma measurements. Based on this methodology, in the present work, the absorbed and effective doses were determined.

In clinical practice, the CBCT procedures are performed with the X-ray tube in continuous motion and, therefore, the irradiation positions may be slightly different from those of the present work because the MCNPX code is designed to simulate the radiation transport with a static radioactive source. In this study a discrete set of 36 point sources (located in 10° steps), was modeled to simulate the actual situation during the exam. This limitation may introduce an additional uncertainty to the results.

To keep the uncertainties in an acceptable range, 10^9 histories were used in each simulated scenario. All simulations were performed using computers with 16 GB of RAM and Intel® Core™ i7 (4 cores) and Intel® Core™ i9 processors (10 cores), using the MCNP *TASKS* option. The simulation time was approximately 48 h with the Intel® Core™ i9 processor.

2.4. Determination of the absorbed and effective doses

The first step to determine the absorbed dose is to obtain a conversion factor (CF), given in particles/mAs. The CF determination is based in the work of Gu et al. (2009) and Stratis et al. (2016). More details about the methodology employed for CF determination was presented elsewhere ((Soares et al., 2019) and references therein). The CF was obtained by equation (1).

$$CF = \frac{K_{air,measured}}{K_{MC,simulated\ per\ particle}} \quad (1)$$

where $K_{air,measured}$ is the air kerma measured experimentally, and $K_{MC,simulated\ per\ particle}$ was determined by the Monte Carlo simulation, at the same experimental conditions.

The second step was to determine the absorbed dose. This quantity was obtained to tissues and organs of the pediatric virtual anthropomorphic phantoms, using Equation (2) (Gu et al., 2009).

$$D_{absorbed\ dose} = D_{simulated} \times CF \times N \quad (2)$$

where $D_{simulated}$ is the F6 tally value (in MeV/g/particle), and N = 1 (number of equipment rotations during the image aquisition).

The third step was to determine the equivalent dose quantity (H_T), using Equation (3).

$$H_T = \omega_R \cdot D_{absorbed\ dose} \quad (3)$$

where ω_R is the radiation weighting factor (for X-rays it equals 1).

The last step was to determine the effective dose (E), according to ICRP 110 (ICRP Publication 110, 2009) recommendation (Equation (4)).

$$E = \sum_T \omega_T H_T \quad (4)$$

where the ω_T is the tissue weighting factor and H_T is the equivalent dose of the organs and tissues for the pediatric anthropomorphic phantoms.

3. Results and discussion

The absorbed and effective doses for the pediatric anthropomorphic phantoms submitted to an i-CAT exam are presented in Tables 1 and 2.

The absorbed doses tend to grow with the field size, which is also observed for the effective doses. This is mainly due to the scattered radiation from the beam, or the fact that the greater field size will encompass more organs than a smaller beam, up to a certain limit, depending on the patient size. The organs with the highest absorbed doses were: thyroid, salivary glands and eyes. This is related to the fact that these organs are being irradiated with the primary radiation beam. The organs with the lowest absorbed doses were: colon, gonads and bladder. Since these organs are far from the region examined, and the beam is collimated, only the scattered radiation reaches them.

In the work of Ludlow and Walker (2013) they concluded that the effective dose results varied according to FOV and field localization. The study was based on the comparison of children and adult anthropomorphic phantoms, undergoing examinations of the i-CAT FLX conical beam (Imaging Sciences, Hatfield, PA). OSL dosimeters were also used for obtaining the doses. The maximum effective dose obtained was 120.1 μSv for the 16 cm × 13 cm FOV, in a 10-year-old child phantom. This value is lower than the maximum effective dose (165.5 μSv) for the 14 cm × 22 cm FOV, obtained in the present work for the 10-year-old phantom. The reasons for this difference are due to the different FOV sizes and the anthropomorphic phantoms utilized. In the present work a virtual phantom, and Monte Carlo simulation were utilized, while in the work of Ludlow and Walker (2013), a physical phantom and experimental measurements were employed. According to them, the effective doses in the child phantoms were, on average, 36% higher than in the adult phantom.

Theodorakou et al. (2012) utilized 10-year-old and adolescent phantoms, with TLD to determine the effective doses during a cone beam CT exam. The maximum effective dose value was 134 μSv for a FOV of 16 cm × 13 cm, tube voltage of 120 kV, considering a Next Generation i-CAT (i-CAT NG) equipment. This value is also lower than the results of the present work, due mainly to the differences such as FOV size, methodology and phantoms utilized.

In the work of Ludlow et al. (2015), they analyzed papers that provided effective dose information on CBCT exams, considering different types of phantoms, methodology and CBCT units. They considered 3 FOV sizes: small FOV (height up to 10 cm), medium FOV (heights 10 - 15 cm) and large FOV (heights larger than15 cm). In their research, they found children effective doses from any protocol, the values ranged from 13 to 769 μSv for large or medium FOVs and 7–521 μSv for small FOVs. Comparing these results (Ludlow et al., 2015) with the results of the present work, the effective dose values are in agreement.

According to the effective dose results shown in Tables 1 and 2, it is possible to observe that the highest effective dose values were obtained for the 5-year-old pediatric virtual anthropomorphic phantom. This phantom has smaller organs, with lower masses, than those from the 10-year-old phantom, leading an increase in the absorbed dose of the organs and tissues.

A comparison with other studies on effective doses in pediatric phantoms, submitted to i-CAT exams, utilizing Monte Carlo simulation, was not possible, because there are no published studies utilizing this methodology. All results found in the literature refer to experimental measurements.

4. Conclusion

In this work the absorbed and effective doses were evaluated for the 5- and 10-year-old virtual anthropomorphic phantoms, during a CBCT exam. For this purpose, these phantoms and an i-CAT equipment were coupled to the MCNPX Monte Carlo code. The absorbed dose values were the highest to organs closer to the primary X-rays beam, such as eye lens, salivary glands and thyroid. The effective dose values increase with the increase of the FOV size, as already presented in experimental works found in the literature. The absorbed and effective doses significantly varied depending on the age of the virtual phantom. The highest effective dose values were obtained for the 5-year-old male virtual anthropomorphic phantom, given its lower organ mass, when compared to the 10-year-old phantom. It is also important to note that the doses delivered to children are much more dangerous than those in adults, since children are more radiosensitive. Specifically during CBCT exams, the use of small or medium FOV sizes is a useful tool to provide the lowest dose values, if they may be applied.

Acknowledgments

The authors would like to thank Dr. Richard Kramer for kindly providing the virtual anthropomorphic phantoms. This work was partially supported by the Brazilian agencies: Fundação de Amparo à Pesquisa do Estado de Minas Gerais (FAPEMIG, Grants No. APQ-03049-15 and APQ-02934-15), Conselho Nacional de Desenvolvimento Científico e Tecnológico (CNPq, Grants No. 421603/2016-0, 420699/2016-3 and 301335/2016-8) and PRPGI/IFBA – Instituto Federal da Bahia.

References

Alkhader, M., Kuribayashi, A., Ohbayashi, N., Nakamura, S., Kurabayashi, T., 2010. Usefulness of cone beam computed tomography in temporomandibular joints with soft tissue pathology. Dentomaxillofacial Radiol. 39, 343–348. https://doi.org/10.1259/dmfr/76385066.

Berdon, W.E., 1999. Editorial commentary on Roebuck D. J.: risk and benefit in paediatric radiology. Pediatr. Radiol. 29, 721–722. https://doi.org/10.1007/s002470050681.

Brenner, D.J., Elliston, C.D., Hall, E.J., Berdon, W.E., 2001. Estimated risks of radiation-induced fatal cancer from pediatric CT. AJR Am. J. Roentgenol. 176, 289–296. https://doi.org/10.2214/ajr.176.2.1760289.

Cassola, V.F., Lima, V.J.D., Kramer, R., Khoury, H.J., 2010a. FASH and MASH: female and male adult human phantoms based on polygon mesh surfaces: I. development of the anatomy. Phys. Med. Biol. 55, 133–162. https://doi.org/10.1088/0031-9155/55/1/009.

Cassola, V.F., Kramer, R., Brayner, C., Khoury, H.J., 2010b. Posture-specific phantoms representing female and male adults in Monte Carlo-based simulations for radiological protection. Phys. Med. Biol. 55, 4399–4430. https://doi.org/10.1088/0031-9155/55/15/014.

Chen, B., Ning, R., 2002. Cone-beam volume CT breast imaging: feasibility study. Med. Phys. 29, 755–770. https://doi.org/10.1118/1.1461843.

Cho, P., Johnson, R.H., Griffin, T.W., 1995. Cone-beam CT for radiotherapy applications. Phys. Med. Biol. 40, 1863–1883. https://doi.org/10.1088/0031-9155/40/11/007.
Dhillon, J., Kalra, G., 2013. Cone beam computed tomography: an innovative tool in pediatric dentistry. Int. J. Paediatr. Dent. 1, 27–31. https://doi.org/10.4103/WKMP-0028.117440.
Dula, K., Mini, R., Lambrecht, J.T., van der Stelt, P.F., Schneeberger, P., Clemens, G., Sanderink, H., Buser, D., 1997. Hypothetical mortality risk associated with spiral tomography of the maxilla and mandible prior to enosseus implant treatment. Eur. J. Oral Sci. 105, 123–129. https://doi.org/10.1111/j.1600-0722.1997.tb00190.x.
Gu, J., Bednarz, B., Caracappa, P.F., Xu, X.G., 2009. The development, validation and application of a multi-detector CT (MDCT) scanner model for assessing organ doses to the pregnant patient and the fetus using Monte Carlo simulations. Phys. Med. Biol. 54, 2699–2717. https://doi.org/10.1088/0031-9155/54/9/007.
Guerrero, M.E., Jacobs, R., Loubele, M., Schutyser, F., Suetens, P., van Steenberghe, D., 2006. State-of-the-art on cone beam CT imaging for preoperative planning of implant placement. Clin. Oral Investig. 10, 1–7. https://doi.org/10.1007/s00784-005-0031-2.
Hall, E.J., Giaccia, A.J., 2006. Radiobiology for the Radiologist. Lippincott Williams & Wilkins, Philadelphia, PA.
Hatcher, D.C., Aboudara, C.L., 2004. Diagnosis goes digital. Am. J. Orthod. Dentofacial Orthop. 125, 512–515. https://doi.org/10.1016/j.ajodo.2003.12.009.
Huda, W., Atherton, J.V., Ware, D.E., Cumming, W.A., 1997. An approach for the estimation of effective radiation dose at CT in pediatric patients. Radiology 203, 417–422. https://doi.org/10.1148/radiology.203.2.9114097.
ICRP Publication 89, 2002. Basic anatomical and physiological data for use in radiological protection reference values. Ann. ICRP 32 (3–4).
ICRP Publication 110, 2009. Adult reference computational phantoms. Ann. ICRP 39 (2).
Imaging Sciences International, 2010. Operator's Manual – Cone Beam Volumetric Tomography and Panoramic Dental Imaging System. Tech. Rep. Part number 990310 – Rev A. Imaging Sciences International, Hatfield, PA.
Kapila, S., Conley, R.S., Harrell, W.E., 2011. The current status of cone beam computed tomography imaging in orthodontics. Dentomaxillofacial Radiol. 40, 24–34. https://doi.org/10.1259/dmfr/12615645.
Kramer, R., Zankl, M., Williams, G., Drexler, G., 1982. The Calculation of Dose from External Photon Exposures Using Reference Human Phantoms and Monte-Carlo Methods. Pt. 1. Tech. Rep. GSF-S-885. Gesellschaft fuer Strahlenund Umweltforschung m.b.H. Muenchen, Neuherberg.
Lee, C., Lodwick, D., Hurtado, J., Pafundi, D., Williams, J.L., Bolch, W.E., 2010. The UF family of reference hybrid phantoms for computational radiation dosimetry. Phys. Med. Biol. 55, 339–363. https://doi.org/10.1088/0031-9155/55/2/002.
Lima, V.J.M., Cassola, V.F., Kramer, R., Lira, C.A.B.O., Khoury, H.J., Vieira, J.W., 2011. Development of 5- and 10-year-old pediatric phantoms based on polygon mesh surfaces. Med. Phys. 38, 4723–4736. https://doi.org/10.1118/1.3615623.
Ludlow, J., Davies-Ludlow, L.E., Brooks, S.L., Howerton, W.B., 2006. Dosimetry of 3 CBCT devices for oral and maxillofacial radiology: CB mercuray, NewTom 3G and i-CAT. Dentomaxillofacial Radiol. 35, 219–226. https://doi.org/10.1259/dmfr/14340323.
Ludlow, J.B., Ivanovic, M., 2008. Comparative dosimetry of dental CBCT devices and 64-slice CT for oral and maxillofacial radiology. Oral Surg. Oral Med. Oral Pathol. Oral Radiol. Endod. 106, 106–114. https://doi.org/10.1016/j.tripleo.2008.03.018.
Ludlow, J.B., Walker, C., 2013. Assessment of phantom dosimetry and image quality of i-CAT FLX cone-beam computed tomography. Am. J. Orthod. Dentofacial Orthop. 144, 802–817. https://doi.org/10.1016/j.ajodo.2013.07.013.
Ludlow, J.B., Timothy, R., Walker, C., Hunter, R., Benavides, E., Samuelson, D.B., Scheske, M.J., 2015. Effective dose of dental CBCT – a meta analysis of published data and additional data for nine CBCT units. Dentomaxillofacial Radiol. 44, 20140197. https://doi.org/10.1259/dmfr.20140197.
Mischkowski, R.A., Pulsfort, R., Ritter, L., Neugebauer, J., Brochhagen, H.G., Keeve, E., Zöller, J.E., 2007. Geometric accuracy of a newly developed cone-beam device for maxillofacial imaging. Oral Surg. Oral Med. Oral Pathol. Oral Radiol. Endod. 104, 551–559. https://doi.org/10.1016/j.tripleo.2007.02.021.
Najjar, A.A., Colosi, D., Dauer, L.T., Prins, R., Patchell, G., Branets, I., Goren, A.D., Faber, R.D., 2013. Comparison of adult and child radiation equivalent doses from 2 dental cone-beam computed tomography units. Am. J. Orthod. Dentofacial Orthop. 143, 784–792. https://doi.org/10.1016/j.ajodo.2013.01.013.
Norris, H., Zhang, Y., Bond, J., Sturgeon, G.M., Minhas, A., Tward, D.J., Ratnanather, J.T., Miller, M.I., Frush, D., Samei, E., Segars, W.P., 2014. A set of 4D pediatric XCAT reference phantoms for multimodality research. Med. Phys. 41, 033701. https://doi.org/10.1118/1.4864238.
Okano, T., Harata, Y., Sugihara, Y., Sakaino, R., Tsuchida, R., Iwai, K., Seki, K., Araki, K., 2009. Absorbed and effective doses from cone beam volumetric imaging for implant planning. Dentomaxillofacial Radiol. 38, 79–85. https://doi.org/10.1259/dmfr/14769929.
Papadimitroulas, P., Kostou, T., Chatzipapas, K., Visvikis, D., Mountris, K.A., Jaouen, V., Katsanos, K., Diamantopoulos, A., Apostolopoulos, D., Balomenos, A., Kopsinis, Y., Loudos, G., Alexakos, C., Karnabatidis, D., Kagadis, G.C., 2018. A review on personalized pediatric dosimetry applications using advanced computational tools. IEEE Trans. Radiat. Plasma Med. Sci (in press). https://doi.org/10.1109/TRPMS.2018.2876562.
Pelowitz, D.B., 2011. MCNPX User's Manual. Version 2.7.0, Report LA-CP-11-0043. Los Alamos National Laboratory, Oak Ridge.
Pierce, D.A., Preston, D.L., 2000. Radiation-related cancer risks at low doses among atomic bomb survivors. Radiat. Res. 154, 178–186. https://doi.org/10.1667/0033-7587(2000)154[0178:RRCRAL]2.0.CO;2.
Robb, R.A., 1982. The dynamic spatial reconstructor: an X-ray videofuoroscopic CT scanner for dynamic volume imaging of moving organs. IEEE Trans. Med. Imaging 1, 22–33. https://doi.org/10.1109/TMI.1982.4307545.
Roberts, J.A., Drage, N.A., Davies, J., Thomas, D.W., 2008. Effective dose from cone beam CT examinations in dentistry. Br. J. Radiol. 82, 35–40. https://doi.org/10.1259/bjr/31419627.
Scaf, G., Lurie, A.G., Mosier, K.M., Kantor, M.L., Ramsby, G.R., Freedman, M.L., 1997. Dosimetry and cost of imaging osseointegrated implants with film-based and computed tomography. Oral Surg. Oral Med. Oral Pathol. Oral Radiol. Endod. 83, 41–48. https://doi.org/10.1016/S1079-2104(97)90089-5.
Scarfe, W.C., Farman, A.G., 2008. What is cone-beam CT and how does it work? Dent. Clin. N. Am. 52, 707–730. https://doi:10.1016/j.cden.2008.05.005.
Schulze, D., Heiland, M., Thurmann, H., Adam, G., 2004. Radiation exposure during midfacial imaging using 4- and 16-slice computed tomography, cone beam computed tomography systems and conventional radiography. Dentomaxillofacial Radiol. 33, 83–86. https://doi.org/10.1259/dmfr/28403350.
Smith-Bindman, R., Lipson, J., Marcus, R., Kim, K.P., Mahesh, M., Gould, R., González, A.B., Miglioretti, D.L., 2009. Radiation dose associated with common computed tomography examinations and the associated lifetime attributable risk of cancer. Arch. Intern. Med. 169, 2078–2086. https://doi.org/10.1001/archinternmed.2009.427.
Soares, M.R., Santos, W.S., Neves, L.P., Perini, A.P., Batista, W.O.G., Belinato, W., Maia, A.F., Caldas, L.V.E., 2019. Dose estimate for cone beam CT equipment protocols using Monte Carlo simulation in computational adult anthropomorphic phantoms. Radiat. Phys. Chem. 155, 252–259. https://doi.org/10.1016/j.radphyschem.2018.06.038.
Stratis, A., Zhang, G., Lopez-Rendon, X., Jacobs, R., Bogaerts, R., Bosmans, H., 2016. Customisation of a Monte Carlo dosimetry tool for dental cone-beam CT systems. Radiat. Protect. Dosim. 169, 378–385. https://doi.org/10.1093/rpd/ncw024.
Theodorakou, C., Walker, A., Horner, K., Pauwels, R., Bogaerts, R., Jacobs, R., 2012. SEDENTEXCT Project Consortium, Estimation of paediatric organ and effective doses from dental cone beam CT using anthropomorphic phantoms. Br. J. Radiol. 85, 153–160. https://doi.org/10.1259/bjr/19389412.
Torres, M.G.G., Campos, P.S.F., Segundo, N.P.N., Ribeiro, M., Navarro, M., Crusoé-Rebello, I., 2010. Evaluation of referential dosages obtained by cone-beam computed tomography examinations acquired with different voxel sizes. Dent. Press J. Orthod. 15, 42–43. https://dx.doi.org/10.1590/S2176-94512010000500008.
Tsiklakis, K., Donta, C., Gavala, S., Karayianni, K., Kamenopoulou, V., Hourdakis, C.J., 2005. Dose reduction in maxillofacial imaging using low dose cone beam CT. Eur. J. Radiol. 56, 413–417. https://doi.org/10.1016/j.ejrad.2005.05.011.
Vos, W.D., Casselman, J., Swennen, G., 2009. Cone-beam computerized tomography (CBCT) imaging of the oral and maxillofacial region: a systematic review of the literature. Int. J. Oral Maxillofac. Surg. 38, 609–625. https://doi.org/10.1016/j.ijom.2009.02.028.
Wall, B.F., Kendall, G.M., Edwards, A.A., Bouffler, S., Muirhead, C.R., Meara, J.R., 2006. What are the risks from medical X-rays and other low dose radiation? Br. J. Radiol. 79, 285–294. https://doi.org/10.1259/bjr/55733882.
Whaites, E., 2006. The biological effects and risks associated with X-rays. In: Whaites, E. (Ed.), Essentials of Dental Radiography and Radiology. Churchill Livingstone Elsevier, London, pp. 488 Ch. 4.